A simplified three-dimensional numerical simulation approach for surface acoustic wave tweezers

Lizhu Liu[1], Jian Zhou[*,1], Kaitao Tan[1], Hui Zhang[2], Xin Yang[3], Huigao Duan[1], YongQing Fu[4]

1. College of Mechanical and Vehicle Engineering, Hunan University, Changsha 410082, China
2. National Engineering Laboratory of Robot Visual Perception and Control Technology, School of Robotics, Hunan University, Changsha, China
3. Department of Electrical and Electronic Engineering, School of Engineering, Cardiff University, Cardiff, CF24 3AA, United Kingdom
4. Faculty of Engineering and Environment, Northumbria University, Newcastle upon Tyne, NE1 8ST, United Kingdom

Corresponding Emails: jianzhou@hnu.edu.cn

Abstract

Standing surface acoustic waves (SSAWs) have been extensively used as acoustic tweezers to manipulate, transport, and separate microparticles and biological cells in a microscale fluidic environment, with great potentials for biomedical sensing, genetic analysis, and therapeutics applications. Currently, there lacks an accurate, reliable, and efficient three-dimensional (3D) modeling platform to simulate behaviors of micron-size particles/cells in acoustofluidics, which is crucial to provide the guidance for the experimental studies. The major challenge for achieving this is the computational complexity of 3D modeling. Herein, a simplified but effective 3D SSAW microfluidic model was developed to investigate the separation and manipulation of particles. This model incorporates propagation attenuation of the surface waves to increase the modeling accuracy, while simplifies the modeling of piezoelectric substrates and the wall of microchannel by determining the effective propagation region of the substrate. We have simulated the SSAWs microfluidics device, and systematically analyzed effects of voltage, tilt angle, and flow rate on the separation of the particles under the SSAWs. The obtained simulation results are compared with those obtained from the experimental studies, showing good agreements. This simplified modeling platform could become a convenient tool for acoustofluidic research.

Keywords: Acoustic tweezers; Microfluidics; Particle separation; Numerical simulation

1. Introduction

Precise manipulation and separation of microparticles and biological cells are critical process steps for biomedical sensing, genetic analysis, and therapeutics applications [1, 2]. With the emergence of lab-on-a-chip [3], many advanced particle-manipulation technologies have been proposed, including hydrodynamic control, plasmonic trap, magnetic tweezers [4], and optical tweezers [5]. However, all these methods have various limitations, such as manipulation scales or the required media, thus restricting their wide-range applications in many biological applications. Acoustic tweezer is a simple, contactless, high-resolution particle-manipulation method that can address many restrictions of other technique. Surface acoustic wave (SAW) based tweezer is one of the important acoustic tweezers [6], and researchers have recently applied SAW tweezers [7] for precise particle manipulation [8], patterning [9, 10], transportation [11], and separation [12]. However, design and experimental studies using these SAW devices and acoustic tweezer platform are quite complicated, which are affected significantly by the coupling of multiple physical fields such as sound pressure field, flow field, and electric field. Simulation and modeling using finite element analysis can provide essential guidance for the experimental work and can effectively reduce the cost of device fabrication and improve the designs. Therefore, it is generally agreed that a low cost and effective simulation model is crucial for the development of SAW microfluidic devices and platform [13].

Early research on simulation models was mainly focused on two-dimensional (2D) numerical modeling. For example, Mao et al studied the transient motions of microparticles using a 2D cross-section simulation, and investigated the impact of boundary vibrations, channel materials, and channel diameters on microparticles' motions [14]. Similarly, some researcher established 2D cross-section simulation to provide the guidance for the design of standing surface acoustic waves (SSAWs) devices. For example, Cynthia et al used 2D cross-section simulations and studied the locations of the pressure lines for a designed multi-stage separation based on the SSAW device [15]. However, these 2D cross-section simulations often did not consider the influence of the fluid fields and the shape of the channel, and they also did not calculate the particles trajectories. Other researchers used simplified planar models to investigate the influences of fluid velocity, input power, and other parameters on particle trajectories [16, 17]. Compared with those based on the cross-section simulations, these planar model can effectively guide the design of microchannel. For example, Shamloo et al used a planar model to design a trapezoidal microchannel to separate the blood cells [18].

2D numerical models have the advantages of less computation complexity, but ignore the deformations and influences of piezoelectric substrates in one direction. In other words, these 2D SAW numerical models [16] have often ineffectively calculated the energy transfer. In addition, in real situations, particle separation or manipulation occur in the 3D space, therefore, 3D SAW simulation will be more suitable for real scenarios and provided more accurate results. Chen et al. proposed a modeling strategy of "slip velocity method" that enabled the 3D simulation of SAW microfluidics in a large domain [19]. However, this method is unsuitable for simulations of the cases within a complex microchannel. Mohammad et al. performed fully-coupled 3D numerical simulations using the SSAWs based on the limiting velocity finite element method [20]. Although their methods could reduce the complexity of computation [20],

they did not consider the propagation attenuation of SAWs and effects of individual parameters on the final separation results.

In this paper, we proposed a simplified but effective 3D numerical simulation for particles separation. Our methodology significantly simplifies the modeling of substrates and microchannels and takes into the account of acoustic propagation attenuation to improve the simulation accuracy [21]. We systematically evaluated the effect of each parameter on the separation outcomes, emphasizing the importance of numerical simulations for experimental guidance. Finally, we fabricated an SSAW device and a tweezer platform based on the simulation results and experimentally validated the accuracy and effectiveness of the model.

2. SSAW acoustofluidic model and governing equations

2.1. 3D numerical SSAW devices models

A typical SSAW microfluidic separation platform is shown in Fig. 1(a). A pair of interdigital transducers (IDTs) are patterned onto a piezoelectric substrate, and a polydimethylsiloxane (PDMS) microfluidic channel is bonded onto the surface of piezoelectric substrate. The working principle is as follows. When RF signals are applied to IDTs, the substrate will vibrate due to the inverse piezoelectric effect, resulting in generation and propagation of Rayleigh SAWs on the substrate [22]. The acoustic waves travel along the surface and are dissipated into the fluid, creating a distribution of acoustic pressure nodes in the fluid [23]. The acoustic pressure in the fluid causes the particles to be subjected to acoustic radiation forces. As the magnitude of the acoustic radiation force is influenced by the particle's radius, it will cause the particles to deviate from their original trajectory and move towards the sound pressure node [24]. In the design shown in Fig. 1(b), as the microchannel is designed at a tilt angle in the middle of IDTs, two particles of different sizes at the outlet could be separated due to different size effects of radiation forces [23].

Under the influence of acoustic radiation force, the movement of particles in the SSAW microfluidic device is complex. Therefore, we have proposed a simplified but effective 3D model to investigate behavior of micron-size particles in acoustofluidics. In this study, the 3D simulation of the SSAW microfluidic device is divided into three modules/steps, i.e., periodic unit simulation, steady-state flow field simulation, and acoustic propagation frequency domain simulation. The proposed specific simulation configuration is shown in Fig. 1(c). The periodic unit of simulation is used to determine the resonant frequency of IDTs. The steady-state flow field simulation is utilized to solve the flow field distribution. The frequency domain simulation of acoustic propagation is used to calculate the results of acoustic pressure distributions. These results are used to provide the initial solutions for the calculation of the particles' motions.

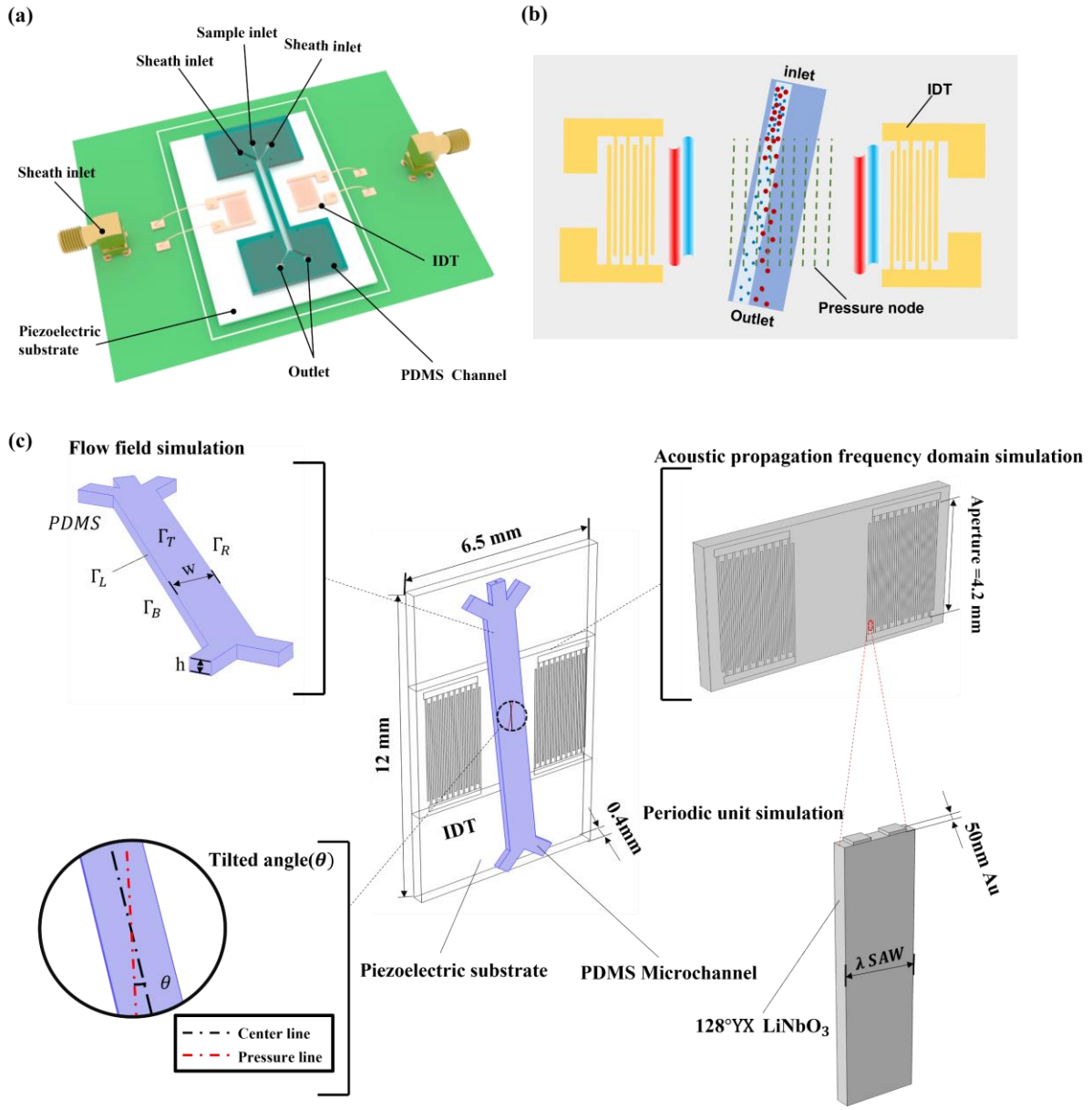

Fig. 1. (a) Schematic of a typical SSAW microfluidic separation device. (b) Separation process from a top view. (c) The composition of 3D numerical model.

2.2. Governing equations for simulations

The motion of particles is guided by the governing equations. In the following, the main governing equations for the simulation are presented. Firstly, the acoustic pressure distribution caused by SAWs in water can be considered as a harmonic problem, which is governed by the Helmholtz wave equation [25]:

$$\nabla^2 p_a - \frac{\omega^2}{u_a^2} p_a = 0 \tag{1}$$

where p_a represents the amplitude of the acoustic pressure, ω represents the angular frequency, and u_a represents the acoustic speed in the flow field.

Assuming the fluid is incompressible, according to the Navier–Stokes (N-S) equation, the

momentum equation can be given as follows [18]:

$$\rho \frac{du_f}{dt} = \rho f - \nabla p + \mu \nabla^2 u_f \tag{2}$$

where p is the pressure, μ is the dynamic viscosity, ρ is the mass density of the fluid medium, and the u_f represents the velocity of the flow field.

According to the standard scattering theory [26], in the region of action of the far-field, the monopole and dipole components are dominant, and thus the acoustic radiation force can be expressed as:

$$F_{rad} = -\pi a^3 * \left[\frac{2\kappa_s}{3} \mathrm{Re}\left[f_0^* * p_a^* \nabla p_a \right] - \rho \mathrm{Re}[f_1^* * v_a^* \nabla v_a] \right] \tag{3}$$

where f_0 represents the monopole scattering coefficient, f_1 represents the dipole scattering coefficient, a represents the radius of particle, Re represents the real part, v_a is the acoustic velocity fields at the particle position, the asterisk represents the conjugate complex, and κ_s is the isentropic compressibility of the fluid medium. According to the derivation in the literature [27], the calculation of f_0 and f_1 can be obtained from the following equations:

$$f_0(\kappa) = 1 - \kappa, \kappa = \frac{\kappa_p}{\kappa_0} \tag{4}$$

$$f_1(\rho, 0) = \frac{2(\rho - 1)}{2(\rho + 1)} \tag{5}$$

According to the N-S formula, the drag force of a spherical particle can be calculated using the following equation:

$$F_{drag} = 6\pi\mu R(u_f - u_p) \tag{6}$$

where u_p is the particle velocity, u_f is the fluid velocity.

Similar to most experimental cases, it is necessary to choose a suitable density of particles to prevent them from sinking down to the bottom of the chamber and make sure the effects of buoyancy and gravity on particle trajectories are minimal. By neglecting gravity and buoyancy forces, the motion of a particle with mass *m* according to Newton's Second Law could be simplified as follow:

$$m_p \frac{dv_p}{dt} = F_{drag} + F_{rad} \tag{7}$$

2.3 Energy attenuation and model simplification

The sheer volume of calculations makes it difficult to build a 3D SAW microfluidic model. For the frequency domain calculations, the large-scale difference between the IDT and the substrate results in an overly dense mesh division, which is a huge task to deal with for the computers. In practical scenarios, due to the wave energy propagation attenuation caused by the PDMS, the affected area of the SAWs on the fluid is limited. This means that the modeling of the piezoelectric substrate that is surrounding the IDTs and also the PDMS can be simplified.

Accordingly, the attenuation of SAW propagation can be estimated via the following equation [21]:

$$\eta = \eta_m \cdot e^{-ad} \tag{8}$$

$$\alpha = \frac{\rho c}{\rho_s c_R \lambda_{saw}} \tag{9}$$

where η_m is the original maximum vibration velocity (generated before contact with the liquid) of the SAW, d is the length of the substrate contact with the medium (such as PDMS and water), α is the attenuation coefficient. ρ and ρ_s represent the density of the medium and substrate (4630 kg/m^3). c and c_R represent the SAW phase velocities in medium and substrate, respectively. According to these equations, we assume that if the length of contact area between the PDMS and substrate is 1 cm and the SAW beam has a wavelength λ of 200 μm, its maximum vibration velocity η will be attenuated to 5% of its original magnitude. This means the SAW energy is focused mainly within the areas covered by the PDMS, whereas outside the IDTs, the wave energy can be ignored (for example the inlet/outlet areas shown in Fig. 1(a)). This is also the reason that some devices have been designed with a cavity in order to reduce the energy attenuation of the SAW propagation. Based on this, we can simplify the modeling of the substrate, and only keep the effective propagation region for frequency domain simulations, which is shown in Fig. 2(a). After this simplification, the number of simulation unit can be reduced to 65% of the original ones (i.e., from 891178 to 584315).

In addition, we proposed to use the calculated attenuation factor α to correct the input power, rather than directly modeling the wall thickness of the microchannel. This can further simplify the model, which is shown in Fig. 2(b). According to the sound energy density and power calculation formula, the vibration velocity of the SAWs is proportional to the input voltage, so the attenuation can be replaced by directly multiplying the coefficient α with the voltage.

2.4 Numerical implementation

Our numerical simulations are carried out using the commercial software COMSOL 5. The $LiNbO_3$ is used as a piezoelectric substrate with a length of 5000 μm, a width of 6500 μm, and a thickness of 400 μm. A pair of IDTs are set on the substrate, each consisting of 20 finger strips with a width of 50 μm, a spacing of 50 μm, a length of 4000 μm, and an overlap length of 3800 μm. The height of microchannel is 200 μm and it consists of the main separation channel, three inlets, and two outlets. Each inlet has a width of 500 μm and a length of 1000 μm. The middle inlet is used as the sample flow entrance. The other two inlets are used as the sheath flow entrances and are set at angles of -45° and 45° to the sample entrance, respectively. The angle between these two outlets is 90°. The length of the two outlets is 1000 μm, and the widths of the two outlets are 300 μm and 500 μm, respectively. Detailed dimensions of the simulation model are shown in Figs. 2(c~d). For the coupling analysis of pressure acoustics, solid mechanics, and electrostatic, the bottom of the substrate is set as a fixed constraint, and half of the IDTs is grounded. A voltage of 16 V is applied to the other half of the IDTs.

The flow rate of the inlet is 3 μl/min, 1 μl/min, and 2 μl/min, respectively (from left to

right). Water is used as the fluid medium. The boundary condition of the wall is assumed as in a no-slip condition, and the impedance value of the wall is 1070 kg/m^3 ×1030 m/s [28] (the density and the acoustic velocity of the PDMS). Particles with diameters of 5 μm and 15 μm are released at the inlet of the flow channels.

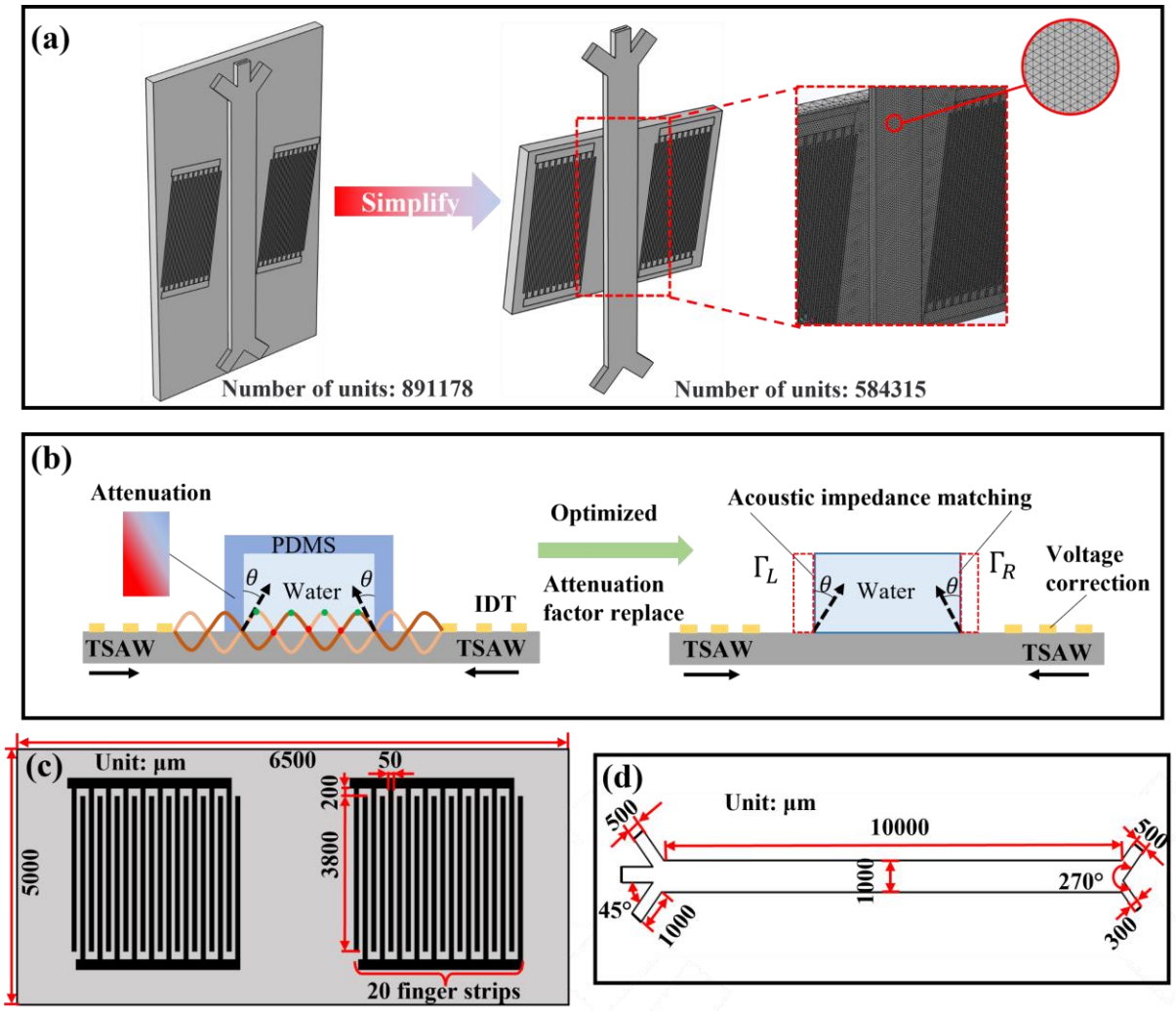

Fig. 2. Simplification of modeling (a) Substrate model simplification; (b) PDMS wall simplification; (c) Detailed dimensions of SAW devices including IDT design; (d) Detailed dimensions of microchannel.

3. Modeling results

3.1 Fluid flow

When the SAW device is applied without any signal input, the main force loaded to the particles is the viscous drag force which is generated by the flowing fluid. In this case, the flow field distribution will be used as the initial solution of the 3D SSAW microfluidic device model, as shown in Fig. 3(a). From the cross-section diagram of the flow velocity, the flow velocity is a variable in the direction of the channel height. However, for the 2D-plane simulation, the particles' distributions at a certain height of the channel and the flow velocity are constants. These results showed that our 3D model contains more information for the state of fluid/particles, compared with the commonly used 2D models. Fig. 3(b) shows the outflow state

of particles without the SAW excitation. All the particles (including both the large and small particles) will flow out of the right outlets, based on the different flow rate of inlets. Therefore, without SAW excitations, particles with different size will not be separated.

3.2 Resonant frequency of Rayleigh waves

To use the SAWs for manipulating and separating microparticles, we need to find their resonant frequency, as the efficiency of energy transfer of SAWs is maximized when the frequency of the input signal is equal to the resonant frequency [29]. Considering the propagation area for sweep frequency will need much more time and computing power, we used periodic unit simulations to find the resonant frequency. As shown in Fig. 3(c), the resonant frequency of the simulated admittance (Y_{11}) for the device in this study is around 19.35 MHz, and the surface vibration pattern of this mode confirms that the wave mode is the Rayleigh wave.

3.3 Acoustic pressure and displacement distribution

When the SAW device is applied with the signal input, the standing SAW (SSAW) will be excited on the $LiNbO_3$ substrate, resulting the acoustic pressure lines well-distributed in the water, as shown in Fig. 3(d). From the enlarged view of the pressure line distribution, the angle between the pressure lines and the flow direction is equals to θ, which is related to the bonding angle (i.e., the tilt angle of IDTs). The particles are driven by the acoustic radiation force (ARF) and are moved to the place of the pressure line. Fig. 3(e) shows the outflow state of particles affected by the ARF. It is clear that, due to the different magnitudes of the ARFs for the particles with different sizes, the 5 μm particles will flow out from the right outlet, whereas the 15 μm particles will be deflected from their original tracks and flow out from the left outlet. That means, with the proper SAW excitation, particles with different sizes can be easily separated due to their different ARFs. Fig. 3(f) shows that the obtained acoustic pressure distributions vary with spatial locations, indicating the three-dimensional distribution of acoustic pressure lines. Results prove that our 3D model can precisely describe the particles' motions and predict the states of particles in their three-dimensional format. In the x-z cross-sectional view of the 3D model, Fig. 3(g) shows the acoustic pressures in the fluid and the Y-direction displacements in the piezoelectric substrate. They show similar distributions with those simulated using the conventional 2D cross-sectional simulation methods [16, 17], and the results agree with those reported in the literature.[30]. These results reveal that our model can correctly predict both the channel structures and the pressure node distribution designs (in the 3D format).

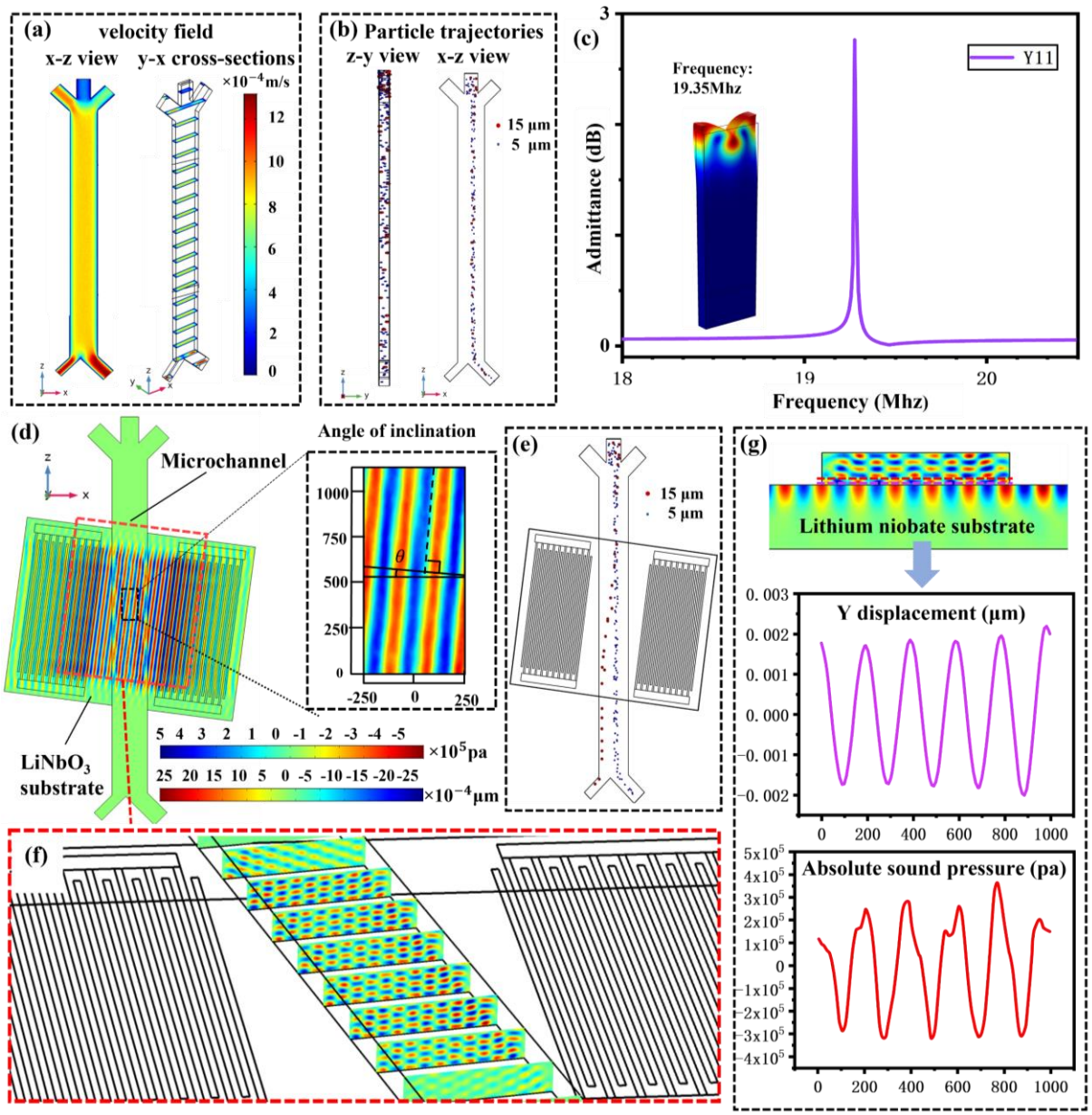

Fig. 3. The 3D simulation of SAW microfluidic device. (a) The velocity field of the fluid. (b) The initial distribution of particles. (c) Surface vibration pattern and Y11 parameter curve. (d) The coupling situation of SAW to the fluid in the 3D model (e) outflow state of particles affected by ARF. (f) The acoustic pressure distribution at different locations in microchannel (g) Distribution of acoustic pressure and y displacement.

4. Simulation of different SSAW designs

After having established the 3D numerical model of the SSAW microfluidic platform, in this section, we will discuss effects of design parameters on acoustofluidic-based particle separations. These parameters include flow rate, voltage, and tilted angle θ. To facilitate analysis, we set the baseline parameters for the simulation as follows, e.g., the entrance flow rates are 3 μl/min, 1 μl/min, and 2 μl/min (from left to right); the input voltage is 16 V, and the tilt angle is 7.5°. The particles' diameters are chosen as 5, 9, 10, 11, 12, and 15 μm, respectively.

The detailed simulation parameters in the following sections are listed in Table 1.

Table1 Summary of parameters used for simulation of particle deflection.

Section	Parameter			
	Input Voltage (V)	Flow rate (μl/min)	Tilted angle, θ, (°)	Frequency (MHz)
4.1	8, 10,12,16,18,20	6	7.5	19.35
4.2	16	3, 6, 12, 24	7.5	19.35
4.3	16	6	2.5,5,7.5,10	19.35
4.4	16	6	7.5	9.95, 15.3, 19.35, 24.875

4.1 Influence of voltage

The voltage affects the amplitude of acoustic pressures in the fluid medium, thus leading to different acoustic pressure distributions and particle deflections for the particles with different sizes. The relationships between the excitation voltages of IDTs and particle trajectories are investigated, and the obtained results are shown in Fig. 4. When the voltage is 8 V, duo to the lower values of ARFs applied on the particles, none of the particles are deflected. With the voltage is increased, the particles begin to deviate from its original trajectories and move to the left outlet. For example, when the voltage is 10 V, the 15 μm particles are quickly deflected and thus separated. As the voltage is further increased, the particles with sizes of 12, 11, 10 and 9 μm are gradually deflected and separated. These results clearly demonstrate that the appropriate increase of voltage can improve the separation efficiency. When the other parameters are the same, for particles of a given size, there is a minimum voltage that these particles can be deflected.

To facilitate analysis, we define the transverse offset of the particle in the SAW propagation region as d_p. We note that with the increase of voltage, the value of d_p for all the particles is gradually increased until the particles contact with the walls of the channel. However, if the voltage is too high (e.g., 20 V), all the particles (except 5 μm) will move onto the pressure line [31], thus resulting in the overlapped trajectories of these particles, as illustrated in Fig. 4(f). In this case, the large particles, e.g., with similar sizes of 9, 10, 11, 12, and 15 μm, cannot be separated. In addition, when the voltage is further increased, vast amount of heat will be produced in the substrate and microchannel. This may result in the formation of bubbles and the disruption of fluid flow [16], both of which will have detrimental effects on the separation effect. Using a high power or a high voltage in the separation applications could cause the damage to the substrate, including the fracture of the devices [16].

Figure 4(g) summarizes the separation distances at different voltages for the particles with different sizes. Results show that the voltage range of 12-16 V is apprpriate for separation applications of multiple-particles, as the distance between each particle trajectories is relatviely large. For particles with diameters of 15 μm and 5 μm, the disitance between different trajectories reach a maximum value at 16 V. Therefore, we choose the 16 V in the following experiments.

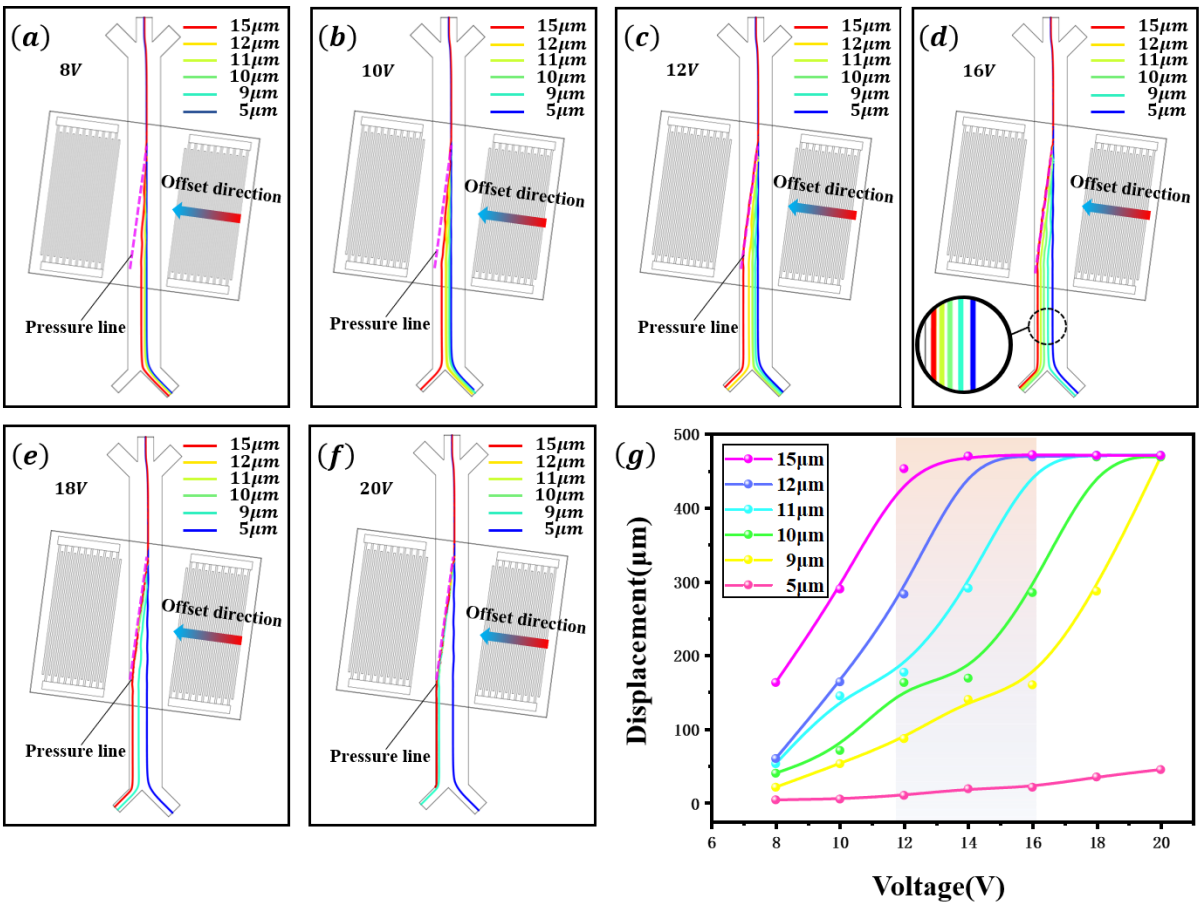

Fig. 4. (a)-(f) Particle trajectories with different volages (8V, 10V, 12V, 16V, 18V, 20V);(g) Relationship between separation distance and input voltage.

4.2 Effects of flow rate

In most realistic scenarios, the SSAW induced separation needs to have high throughputs to improve the separation efficiency [32]. Therefore, we further explore the effect of input flow rate on the simulation results. Fig. 5(a) shows that there is no particle deflection when the SAW device is applied with a high flow rate (e.g., 24 μl/min). This is because at such a high flow rate, the ARFs can't overcome the drag force, which will eventually lead to the failure of separation. To ensure that particles are sufficiently affected by the ARF, the flow velocity should be properly reduced. As the input flow rate is decreased, the d_p values of the particles are increased. For example, when the input flow rate is decreased to 12 μl/min, the particles of 15 μm begin to be separated from the original trajectory. When the input flow rate is further decreased to 3 μl/min, all the particles with sizes of 15, 12, 11, 10 and 9 μm are separated from the original trajectory. These results clearly show that reducing the flow rate is advantageous for separating small particles due to their increased times under the SSAW field.

However, if the flow rate is too low, the trajectories of large particles with similar sizes may be highly overlapped, as shown in Fig. 5(d). This is because the excessively decreased flow rate will significantly increase the time for the particles to pass through the channel, and finally be moved along the same line. We have summarized the effects of separation distance at different average flow rates, and the obtained results show that when the input flow rate is between 6-12 μl/min, the d_p values of different particle trajectories are significantly different,

thus it is more suitable for separating the particles with similar sizes. When the separation efficiency is reached, a larger flow rate is preferred to achieve a high throughput. Therefore, we choose a flow rate of 6 μl/min for the separation of 5 and 15 μm particles in the subsequent experiments, to ensure a large deviation distance and high throughput separation.

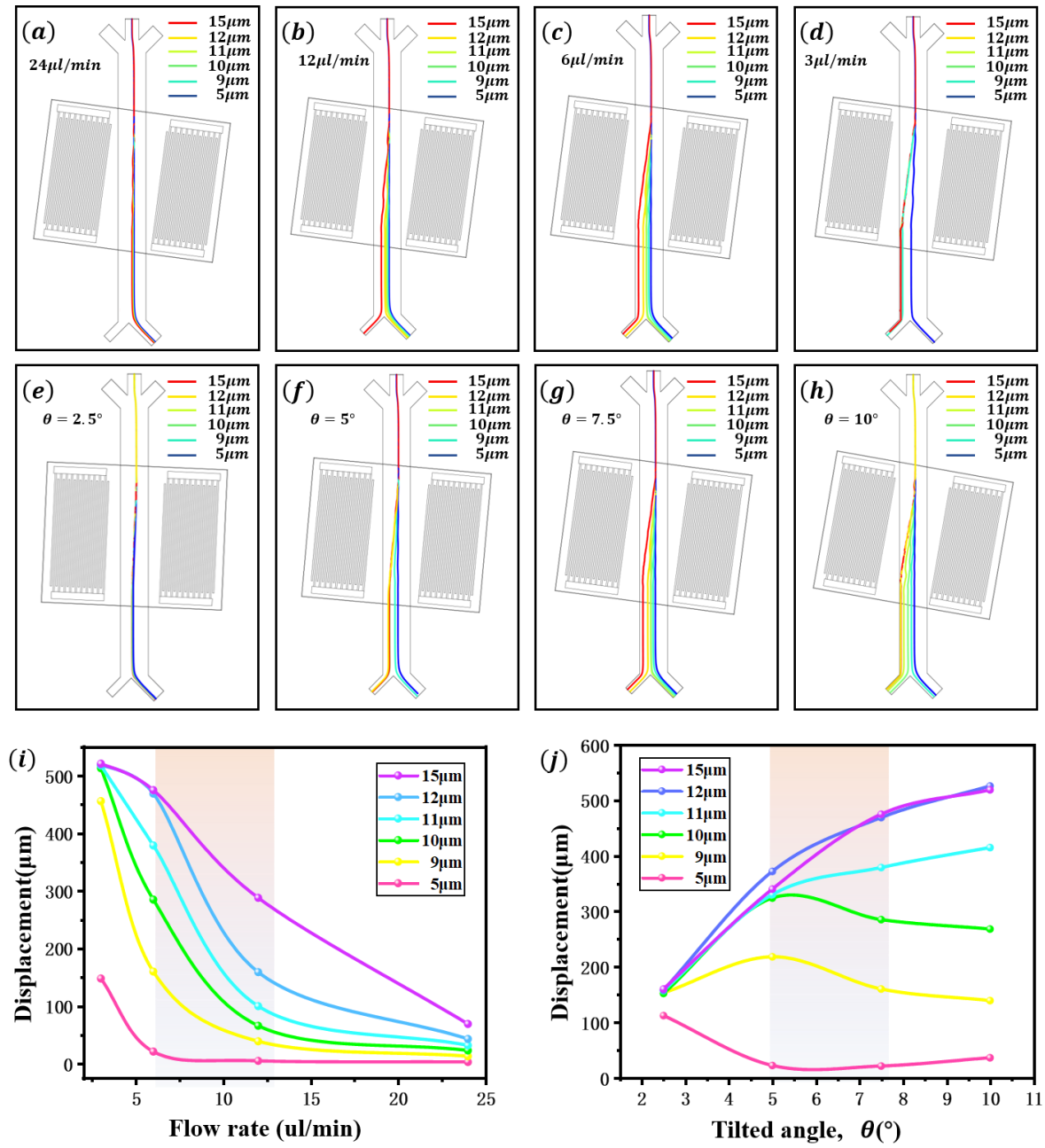

Fig. 5. (a)-(d) Particle trajectories at a different tilted angle (2.5°, 5°, 7.5°, 10°). (e)-(h) Particle trajectories at a different flow rate (3 μl/min, 6 μl/min, 12 μl/min, 24 μl/min). (i) Separation distance at different flow rate. (j) Separation distance at different tilted angles.

4.3 Influence of tilted angle

The tilted angle of channel vs. IDT direction is also an important design parameter of the SSAW device. Adjusting the tilt angle will change the distributions of the pressure lines and cause the particles to move at a different angle. Figs. 5(e~h) show that if the particles have a smaller size (e.g., 5 μm), the change of their trajectory is insignificant with the increase of angle

θ, mainly due to the weak ARFs. Whereas the particles with a larger size (e.g., 15 μm) will show significantly changed trajectory with the change of the tilted angle. Fig. 5(j) summarizes the separation distances at different tilt angles for particles with different sizes. Results clearly show that the distance among the particle's trajectories tends to increase as the tilt angle is increased, hence a large tilt angle is beneficial for multi-size separations. However, increasing the tilt angle does not always increase the deflected distance of particles. As illustrated in Fig. 5 (j), the d_p of particles with sizes of 9 and 10 μm is increased initially but then reduced as the tilt angle is further increased. The reason for this is that as the tilt angle is increased, the component of ARFs that compete with drag force increases, while the component of ARFs that induces a lateral deflection becomes decreased [33]. In addition, a larger tilt angle will increase the chip size, which is not beneficial for the integration and miniaturization. Taking these considerations into account, we choose the tilt angle range of 5-7.5° for separating the 5 and 15 μm particles in our experiments.

4.4. Influence of SAW frequency

The resonance frequency is also a significant parameter for SAW separation. Changing the resonant frequency will modify the width of the acoustic pressure lines. In this paper, we study the influence of the resonant frequency by changing the width of the IDT fingers. The SAW devise with finger widths of 100, 65, 50, and 40 μm have their corresponding resonance frequencies of 9.95, 15.3, 19.35, and 24.875 MHz, respectively. Figure 6(a) shows that only 15 μm size particles are separated when the SAW device is applied under a lower frequency (e.g., 10 MHz). This is because applying a low frequency signal will generate low density of acoustic wave energy, which is ineffective to shift smaller particles. With the same input power, the particles with sizes of 12, 11, 10, and 9 μm are also deflected and separated with increasing the frequency, as shown in Figs. 6(b~d). Therefore, increasing frequency is beneficial for separating smaller sizes of particles, thus significantly reducing the need for high power input, which is consistent with the previous experimentally obtained results [34, 35]. However, too much higher resonant frequency means that it will need to significantly reduce the device's size and thus the manufacturing process becomes challenging. Taking these considerations into account, we choose the resonance frequency range of 15~25 MHz for separating the 5 and 15 μm particles in our experiments.

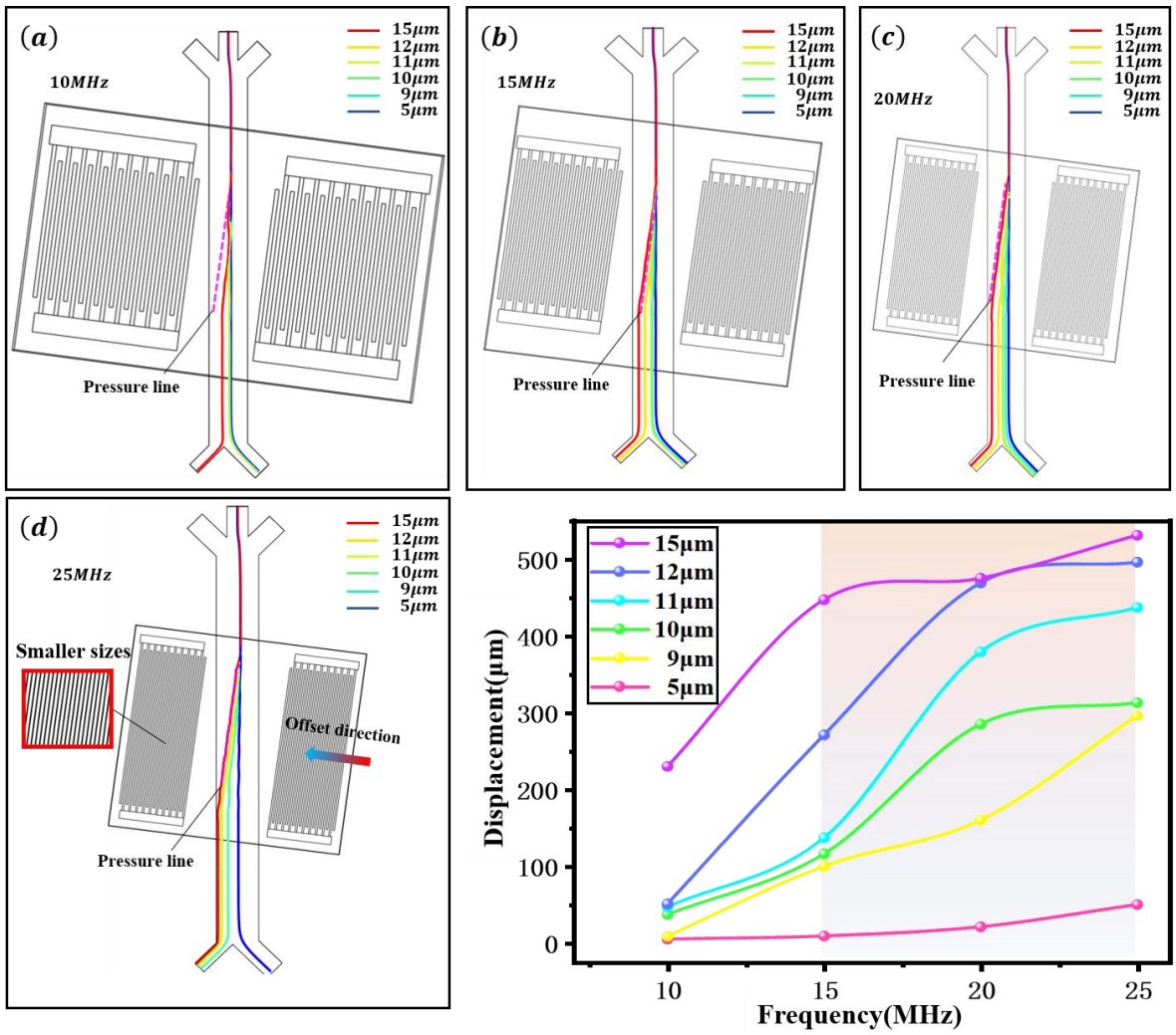

Fig. 6. (a)-(d) Particle trajectories with different resonant frequency (9.95 MHz, 15.3 MHz, 19.35 MHz, 24.875 MHz.) (e) Relationship between separation distance and resonant frequency.

5. Particle tracing and model verification

To verify our proposed new platform of 3D numerical simulations, we fabricated the SSAW microfluidic platform. The fabrication process involves three major steps: (i) fabrication of the IDTs on a $LiNbO_3$ piezoelectric substrate; (ii) fabrication of PDMS microchannel; and (iii) bonding of the PDMS channel onto the $LiNbO_3$ piezoelectric substrate with IDTs. Photolithography, metal deposition, and lift-off processes were used to fabricate the SAW IDTs. Double-layer metals (Cr/Au with their thicknesses of 20/80 nanometers) were used as the materials of the IDTs. The PDMS microchannels were fabricated using a mold-replica technique. Finally, the IDT substrate and the PDMS microchannel are both treated with oxygen plasma and bonded together with a tilting angle of 7.5°. Figure 7(a) shows the prepared SSAW microfluidic device, and its enlarged view clearly shows the IDT structure (Fig. 7(b)). To characterize the fabricated SAW device, a vector network analyzer is used to characterize the reflection spectrum of the SAW device off load and on load with PDMS, The obtained results are shown in Fig. 7(c), which indicates that the resonant frequency of the fabricated device is consistent with the simulation results.

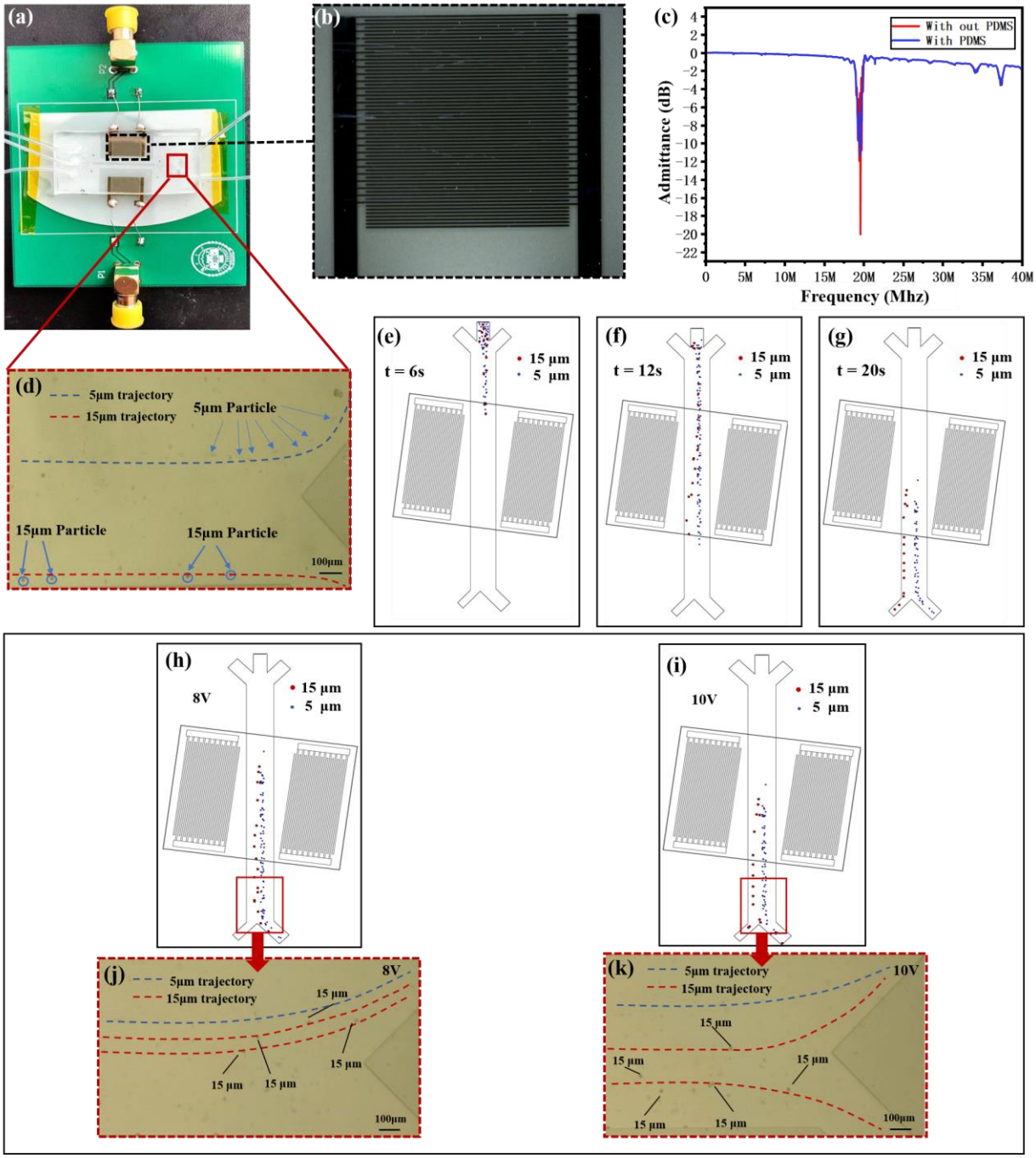

Fig. 7. Model verification process. (a) Photo showing a SSAW separation device. (b) zoomed-in view IDT structure (c) The S11 parameter of the device (d) Experimental observations at optical parameters (e)-(g) The particles trajectories at different times (h)-(i) Experimental observation with different volage input (8V, 10V). (j)-(k) Predicted trajectories with different volage input.

Using the fabricated SSAW device under the optimized parameters (e.g., a flow rate of 6 μl/min, a tilted angle of 7.5°, a voltage of 16 V, and the particles sizes of 5 and 15 μm), the separation results are shown in Fig. 7(d). The larger size particles (15 μm) are collected in the upper outlet channel whereas the small ones (5 μm) are accumulated in the lower outlet.

Experimental results are in good agreements with simulated ones (Figs. 7(e~g)), thus verifying the accuracy of our proposed 3D simulation platform. Our device can process 120 particles (with diameter of 15 μm) per minute, and our best experimental separation accuracy rate (the separated numbers/total numbers) is ~93.54%.

To further valid the correctness of the developed platform, we compare the results of the simulation and the experiment results with the applied voltages set to be 8 V and 10 V. In the experiments, when the voltage is set to be 8 V, most of 15 μm particles flow out of the same outlet, which is similar to that of 5 μm particles. In this case, the 15 μm particles could not be separated from the initial trajectories. As the voltage is increased to 10 V, some 15 μm particles are moved towards the wall of the channel and are separated from the 5 μm particles. These experiment results match well with the predicted trajectories obtained using the simulations, as shown in Figs. 7(h~k). Based on these results, we conclude that our proposed 3D simulation platform is reliable, which has the potential to provide the guidance for the experimental results.

In addition, to perform qualitative analysis between the simulation and experiment results, we estimate the average transverse offsets of the 15 μm particle. Under the optimal parameters (e.g., a flow rate of 6 μl/min, a tilted angle of 7.5°, a voltage of 16 V, and the particles sizes of 5 and 15 μm), the average offsets of experiment and simulation results are 457 μm and 473 μm, respectively, with an error rate less than 4%. With the voltage decreased to 10 V, the average offsets of the experiment and simulation results are decreased to 324 μm and 342 μm, respectively, with an error rate of 5.2%. When the voltage is further decreased to 8 V, the average offsets of the experiment and simulation results are decreased to 136 μm and 150 μm, respectively, with an error rate of 10%. Based on the above discussion, we can conclude that the simulation can be used to predict the performance of SAW tweezers, which was confirmed by the qualitative experimental results. With the volage decreased, the error rates of the average transverse offsets are increased gradually, which may be related to the mesh issues and the complex experimental conditions.

6. Conclusions

In this paper, a simplified but effective 3D SSAW microfluidic model was developed to investigate the separation and manipulation of particles. The model incorporates SAW propagation attenuation to increase accuracy and simplifies the modeling of piezoelectric substrates and the wall of microchannel by determining the effective propagation region of the substrate. We have simulated the SSAWs using the microfluidics device with the different tilting angles of the microchamber with the IDTs. Effects of voltage, tilt angle, and flow rate on the separation of the particles are modeled and systematically analyzed, and the obtained results are compared with those obtained from the experimental studies, which show good agreements. This simplified model could become a convenient tool for designing acoustofluidic devices.

ACKNOWLEDGMENTS

This work was supported by the General Program of National Natural Science Foundation of China (NSFC No.52075162), The Innovation Leading Program of New and High-tech Industry of Hunan Province(2020GK2015, 2021GK4014),The Natural Science Foundation of Hunan

Province (2021JJ20018), Joint fund of the Ministry of Education (Young talents), the Key Research Project of Guangdong Province (2020B0101040002), the Natural Science Foundation of Changsha (kq2007026), the Engineering Physics and Science Research Council of UK (EPSRC EP/P018998/1) and International Exchange Grant (IEC/NSFC/201078) through Royal Society and the NSFC.

References

[1] M. Wu, A. Ozcelik, J. Rufo, Z. Wang, R. Fang, T.J. Huang, Acoustofluidic separation of cells and particles, Microsystems & nanoengineering, 5 (2019) 1-18.

[2] H. Cho, J. Kim, C.W. Jeon, K.-H. Han, A disposable microfluidic device with a reusable magnetophoretic functional substrate for isolation of circulating tumor cells, Lab on a Chip, 17 (2017) 4113-4123.

[3] M.H. Mohammadi, S. Mulder, P. Khashayar, A. Kalbasi, M. Azimzadeh, A.R. Aref, Saliva Lab-on-a-chip Biosensors: recent novel ideas and applications in disease detection, Microchem. J., 168 (2021) 106506.

[4] A.R. Bausch, W. Möller, E. Sackmann, Measurement of local viscoelasticity and forces in living cells by magnetic tweezers, Biophys. J., 76 (1999) 573-579.

[5] S. Zhang, M. Elsayed, R. Peng, Y. Chen, Y. Zhang, J. Peng, W. Li, M.D. Chamberlain, A. Nikitina, S. Yu, Reconfigurable multi-component micromachines driven by optoelectronic tweezers, Nat. Commun., 12 (2021) 1-9.

[6] Y.Q. Fu, J. Luo, N.-T. Nguyen, A. Walton, A.J. Flewitt, X.-T. Zu, Y. Li, G. McHale, A. Matthews, E. Iborra, Advances in piezoelectric thin films for acoustic biosensors, acoustofluidics and lab-on-chip applications, Progress in Materials Science, 89 (2017) 31-91.

[7] P. Li, Z. Mao, Z. Peng, L. Zhou, Y. Chen, P.-H. Huang, C.I. Truica, J.J. Drabick, W.S. El-Deiry, M. Dao, Acoustic separation of circulating tumor cells, Proceedings of the National Academy of Sciences, 112 (2015) 4970-4975.

[8] A. Barani, H. Paktinat, M. Janmaleki, A. Mohammadi, P. Mosaddegh, A. Fadaei-Tehrani, A. Sanati-Nezhad, Microfluidic integrated acoustic waving for manipulation of cells and molecules, Biosens. Bioelectron., 85 (2016) 714-725.

[9] X. Tao, T. Dai Nguyen, H. Jin, R. Tao, J. Luo, X. Yang, H. Torun, J. Zhou, S. Huang, L. Shi, 3D patterning/manipulating microparticles and yeast cells using ZnO/Si thin film surface acoustic waves, Sensors and Actuators B: Chemical, 299 (2019) 126991.

[10] T.D. Nguyen, V.T. Tran, Y.Q. Fu, H.J.A.P.L. Du, Patterning and manipulating microparticles into a three-dimensional matrix using standing surface acoustic waves, 112 (2018) 213507.

[11] L. Meng, F. Cai, J. Chen, L. Niu, Y. Li, J. Wu, H. Zheng, Precise and programmable manipulation of microbubbles by two-dimensional standing surface acoustic waves, Appl. Phys. Lett., 100 (2012) 173701.

[12] G. Destgeer, B.H. Ha, J.H. Jung, H.J. Sung, Submicron separation of microspheres via travelling surface acoustic waves, Lab on a Chip, 14 (2014) 4665-4672.

[13] S. Maramizonouz, M. Rahmati, A. Link, T. Franke, Y. Fu, Numerical and experimental studies of acoustic streaming effects on microparticles/droplets in microchannel flow, International Journal of Engineering Science, 169 (2021) 103563.

[14] Z. Mao, Y. Xie, F. Guo, L. Ren, P.-H. Huang, Y. Chen, J. Rufo, F. Costanzo, T.J. Huang, Experimental and numerical studies on standing surface acoustic wave microfluidics, Lab on a Chip, 16 (2016) 515-524.
[15] A. Shamloo, M. Boodaghi, Design and simulation of a microfluidic device for acoustic cell separation, Ultrasonics, 84 (2018) 234-243.
[16] T. Peng, M. Zhou, S. Yuan, C. Fan, B. Jiang, Numerical investigation of particle deflection in tilted-angle standing surface acoustic wave microfluidic devices, Applied Mathematical Modelling, 101 (2022) 517-532.
[17] A.M. Soliman, M.A. Eldosoky, T.E. Taha, The separation of blood components using standing surface acoustic waves (SSAWs) microfluidic devices: analysis and simulation, Bioengineering, 4 (2017) 28.
[18] A. Shamloo, F.Y. Parast, Simulation of blood particle separation in a trapezoidal microfluidic device by acoustic force, IEEE Trans. Electron Devices, 66 (2019) 1495-1503.
[19] C. Chen, S.P. Zhang, Z. Mao, N. Nama, Y. Gu, P.-H. Huang, Y. Jing, X. Guo, F. Costanzo, T.J. Huang, Three-dimensional numerical simulation and experimental investigation of boundary-driven streaming in surface acoustic wave microfluidics, Lab on a Chip, 18 (2018) 3645-3654.
[20] Namnabat, Mohammad Sadegh, Mahdi Moghimi Zand, and Ehsan Houshfar, 3D numerical simulation of acoustophoretic motion induced by boundary-driven acoustic streaming in standing surface acoustic wave microfluidics, Scientific Reports 11 (2021): 1-16.
[21] M.B. Dentry, L.Y. Yeo, J.R. Friend, Frequency effects on the scale and behavior of acoustic streaming, Physical Review E, 89 (2014) 013203.
[22] S.-C.S. Lin, X. Mao, T.J. Huang, Surface acoustic wave (SAW) acoustophoresis: now and beyond, Lab on a Chip, 12 (2012) 2766-2770.
[23] F. Guo, Z. Mao, Y. Chen, Z. Xie, J.P. Lata, P. Li, L. Ren, J. Liu, J. Yang, M. Dao, Three-dimensional manipulation of single cells using surface acoustic waves, Proceedings of the National Academy of Sciences, 113 (2016) 1522-1527.
[24] D. Hartono, Y. Liu, P.L. Tan, X.Y.S. Then, L.-Y.L. Yung, K.-M. Lim, On-chip measurements of cell compressibility via acoustic radiation, Lab on a Chip, 11 (2011) 4072-4080.
[25] J. Lei, F. Cheng, K. Li, Z. Guo, Numerical simulation of continuous separation of microparticles in two-stage acousto-microfluidic systems, Applied Mathematical Modelling, 83 (2020) 342-356.
[26] N. Nama, R. Barnkob, Z. Mao, C.J. Kähler, F. Costanzo, T.J. Huang, Numerical study of acoustophoretic motion of particles in a PDMS microchannel driven by surface acoustic waves, Lab on a Chip, 15 (2015) 2700-2709.
[27] J. Guo, Y. Kang, Y. Ai, Radiation dominated acoustophoresis driven by surface acoustic waves, J. Colloid Interface Sci., 455 (2015) 203-211.
[28] Z. Ni, C. Yin, G. Xu, L. Xie, J. Huang, S. Liu, J. Tu, X. Guo, D. Zhang, Modelling of SAW-PDMS acoustofluidics: Physical fields and particle motions influenced by different descriptions of the PDMS domain, Lab on a Chip, 19 (2019) 2728-2740.
[29] W. Connacher, N. Zhang, A. Huang, J. Mei, S. Zhang, T. Gopesh, J. Friend, Micro/nano acoustofluidics: materials, phenomena, design, devices, and applications, Lab on a Chip, 18

(2018) 1952-1996.
[30] Z. Ni, C. Yin, G. Xu, L. Xie, J. Huang, S. Liu, J. Tu, X. Guo, D.J.L.o.a.C. Zhang, Modelling of SAW-PDMS acoustofluidics: Physical fields and particle motions influenced by different descriptions of the PDMS domain, 19 (2019) 2728-2740.
[31] S. Zhao, M. Wu, S. Yang, Y. Wu, Y. Gu, C. Chen, J. Ye, Z. Xie, Z. Tian, H.J.L.o.a.C. Bachman, A disposable acoustofluidic chip for nano/microparticle separation using unidirectional acoustic transducers, 20 (2020) 1298-1308.
[32] K. Wang, W. Zhou, Z. Lin, F. Cai, F. Li, J. Wu, L. Meng, L. Niu, H. Zheng, Sorting of tumour cells in a microfluidic device by multi-stage surface acoustic waves, Sensors and Actuators B: Chemical, 258 (2018) 1174-1183.
[33] X. Ding, Z. Peng, S.-C.S. Lin, M. Geri, S. Li, P. Li, Y. Chen, M. Dao, S. Suresh, T.J.J.P.o.t.N.A.o.S. Huang, Cell separation using tilted-angle standing surface acoustic waves, 111 (2014) 12992-12997.
[34] M. Wu, Y. Ouyang, Z. Wang, R. Zhang, P.H. Huang, C. Chen, H. Li, P. Li, D. Quinn, M. Dao, S. Suresh, Y. Sadovsky, T.J. Huang, Isolation of exosomes from whole blood by integrating acoustics and microfluidics, Proc. Natl. Acad. Sci. U. S. A. 114 (2017) 10584 10589,
[35] Z. Wang, F. Li, J. Rufo, C. Chen, S. Yang, L. Li, J. Zhang, J. Cheng, Y. Kim, M. Wu, E. Abemayor, M. Tu, D. Chia, R. Spruce, N. Batis, H. Mehanna, D.T.W. Wong, T.J. Huang, Acoustofluidic salivary exosome isolation: a liquid biopsy compatible approach for human papillomavirus–associated oropharyngeal cancer detection, J. Mol. Diagnostics 22 (2020) 50–59